Title

Impacts of climate warming on the frozen ground and eco-hydrology in the Yellow River source region, China

Authors

Qin, Yue

Yang, Dawen

Gao, Bing

et al.

Publication Date

2017-12-01

DOI

10.1016/j.scitotenv.2017.06.188

Peer reviewed

Impacts of climate warming on the frozen ground and eco-hydrology in the Yellow River source region, China

Yue Qin[ab] Dawen Yang[a] Bing Gao[c] Taihua Wang[a] Jinsong Chen[b] Yun Chen[d] Yuhan Wang[a] Guanheng Zheng[a]

Abstract

The Yellow River source region is located in the transition region between permafrost and seasonally frozen ground on the northeastern Qinghai-Tibet Plateau. The region has experienced severe climate change, especially air temperature increases, in past decades. In this study, we employed a geomorphology-based eco-hydrological model (GBEHM) to assess the impacts of climate change on the frozen ground and eco-hydrological processes in the region. Based on a long-term simulation from 1981 to 2015, we found that the areal mean maximum thickness of seasonally frozen ground ranged from 1.1–1.8 m and decreased by 1.2 cm per year. Additionally, the ratio of the permafrost area to the total area decreased by 1.1% per year. These decreasing trends are faster than the average in China because the study area is on the sensitive margin of the Qinghai-Tibet Plateau. The annual runoff exhibited variations similar to those of the annual precipitation (R^2 = 0.85), although the annual evapotranspiration (ET) exhibited an increasing trend (14.3 mm/10 a) similar to that of the annual mean air temperature (0.66 °C/10 a). The runoff coefficient (annual runoff divided by annual precipitation) displayed a decreasing trend because of the increasing ET, and the vegetation responses to climate warming and permafrost degradation were manifested as increases in the leaf area index (LAI) and ET at the start of the growing season. Furthermore, the results showed that changes to the frozen ground depth affected vegetation growth. Notably, a rapid decrease in the frozen ground depth (< − 3.0 cm/a) decreased the topsoil moisture and then decreased the LAI. This study showed that the eco-hydrological processes in the headwater area of the Yellow River have changed because of permafrost degradation, and these changes could further influence the water resourcesavailability in the middle and lower reaches of the basin.

Graphical abstract

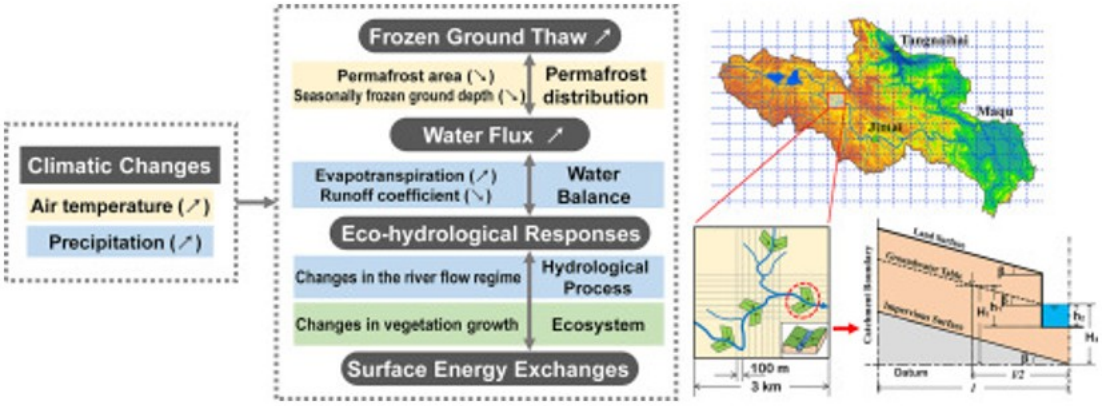

Keywords: Distributed eco-hydrological model, Frozen ground, Climate change, Hydrological processes, Yellow River

1. Introduction

As air temperature continuously increases in the cold season in many regions of the world, the effects of climate warming on water resources and ecosystems have become an important issue in several recent studies (Immerzeel et al., 2010, Bartos and Chester, 2015, Belmecheri et al., 2016). The warming trend in the mid-latitude arid regions is more enhanced than the global average (Huang et al., 2012), and this trend leads to remarkable impacts on the water cycle and fragile ecosystems (Rotenberg and Yakir, 2010). Moreover, climate warming could accelerate permafrost degradation and cause regional hydrological changes (Jin and Li, 2009, Bense et al., 2012, Cheng and Jin, 2013). It has become increasingly interesting to understand how climate change affects the frozen ground and regional eco-hydrology.

Frozen ground, including permafrost and seasonally frozen ground, has been recognized as a sensitive indicator of climate change. The hydrological effects of frozen ground changes caused by climate warming have been discussed in previous studies (Koren et al., 1999, Woo et al., 2000, Zhang et al., 2007). Many data-based studies have investigated the long-term changes in streamflow, and the results indicated that the baseflow has increased in the permafrost basins in northern Canada (Walvoord and Striegl, 2007), northern Eurasia (Smith et al., 2007), northeastern China (Duan et al., 2017a, Duan et al., 2017b), and northwestern China (Qin et al., 2016). The physical processes underlying frozen ground changes, such as changes in

the soil water content, increases in the soil hydraulic conductivity, and redistributions of the frozen and thawed water, can be quantitatively simulated using process-based models (Walvoord and Kurylyk, 2016). Frozen ground changes can also affect the vegetation activity in cold regions. For instance, frozen ground has been considered an important factor for vegetation growth at the start of the growing seasonbecause it affects the stomatal conductance of leaves (Cable et al., 2014), soil temperature(Iijima et al., 2014), topsoil moisture (Cuo et al., 2015) and soil organic carbon (Mu et al., 2015).

Most previous studies of the changes in frozen ground have used in situ observations, empirical or statistical models, and process-based models. In situ observations of the air temperature, soil temperature, frozen ground depth and groundwater table depth have frequently been collected (Frauenfeld and Zhang, 2011, Cheng and Jin, 2013, Hubbard et al., 2013, Oliva et al., 2016, Chaves et al., 2017), although spatio-temporally continuous changes in frozen ground are not fully reflected by these data because of the limited site number and observation duration. In studies based on empirical or statistical models, the freezing index, thawing index, Stefan Solution and Kudryavtsev Equation have been applied to upscale site observations to regional results (Pang et al., 2012, Wu et al., 2015, Peng et al., 2017). However, water and heat transfer in frozen soil is generally neglected in empirical or statistical methods, and models must be well calibrated because most parameters are not physically based. In studies that used process-based models, frozen soil parameterization has been incorporated into the distributed hydrological models, such as WEB-DHM (Wang et al., 2010), MIKE-SHE (Bosson et al., 2012) and VIC (Cuo et al., 2015). However, most previous studies considered the frozen soil layer a static and impermeable or low permeability layer, and dynamic frozen ground changes and the associated impacts on regional eco-hydrology were not well evaluated.

The northern and eastern margins of the Qinghai-Tibet Plateau are the source regions of major rivers in East Asia. The Yellow River source region has been studied in recent years to understand the effects of climate change (Jin et al., 2009, Hu et al., 2011, Cuo et al., 2013). Frozen ground changes in the Yellow River source region have been analyzed in previous studies using meteorological observations at the point scale (Jin et al., 2009, Zhang et al.,

2009). However, the impacts of frozen ground changes on vegetation growth are not fully understood. The spatio-temporal changes to frozen ground and the eco-hydrological responses to these changes remain unclear in the Yellow River source region.

The objectives of this study are as follows: (i) to understand the impacts of climate warming on frozen ground; (ii) to reveal the spatio-temporal variations in the water balancecomponents; and (iii) to analyze the relationships among the frozen ground changes, vegetation growth and hydrology in the Yellow River source region over the past 35 years.

2. Study area and data

2.1. Yellow River source region

The Yellow River, which originates from the northeastern Qinghai-Tibet Plateau (see Fig. 1), is the second longest river in China with a total length of 5464 km (Cong et al., 2009). The Yellow River source region, i.e., the region upstream of Tangnaihai (TNH) hydrological station, has a drainage area of 123,700 km^2. The Yellow River source region is located in the transition region between seasonally frozen ground and permafrost, and the boundaries between seasonally frozen ground and permafrost are changing due to increases in temperature (Jin et al., 2009). The elevation of the Yellow River source region ranges from 2650 m to 6250 m above sea level (a.s.l.). The main vegetation types are alpine meadow and steppe in the plain area and sparse vegetation in the high mountains above 4800 m a.s.l. (Jin et al., 2009).

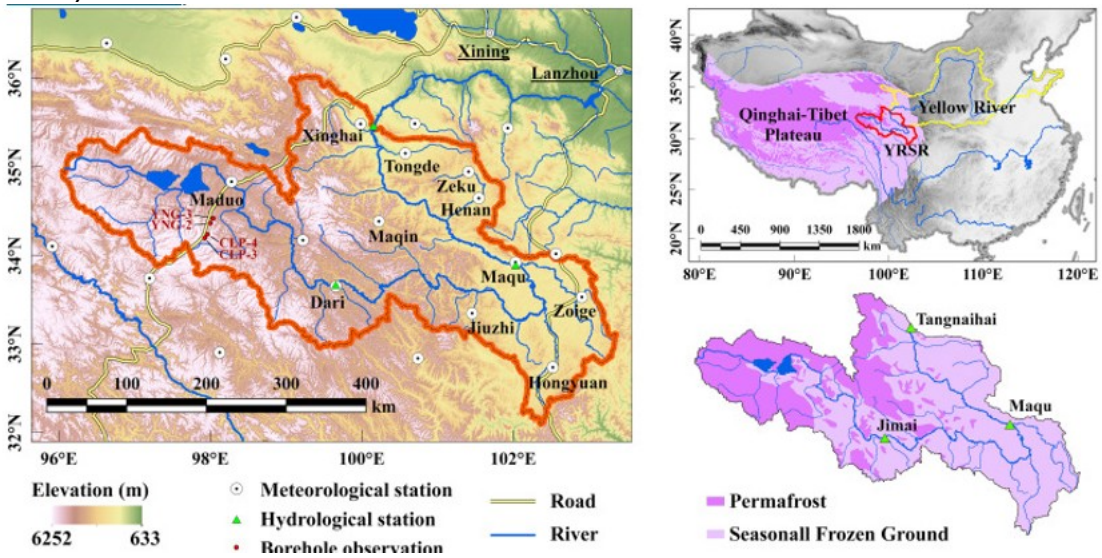

Fig. 1. Locations of the Yellow River source region (YRSR) and observation stations. The frozen groundtypes (permafrost or seasonally frozen ground) are shown in sub-figures.

2.2. Data

Data used in this study include geographic information for model construction, climatic forcing data and other observed data for model validation. Table 1 lists the datasets used in this study and their sources.

Table 1. Parameters and data used to drive the model or validate the simulations.

Type	Parameter	Original resolution	Value range	Unit	Source
Climatic forcing data	Air temperature (mean, maxima and minima)	Daily at 22 stations	–	°C	China Meteorological Administration (http://data.cma.cn)
	Precipitation		–	mm	
	Average wind speed		–	$m\ s^{-1}$	
	Average relative humility		–	%	
	Sunshine duration		–	hour	
Soil parameters	Saturated soil moisture	One-time and 0.00833° × 0.00833°	[0.413, 0.650]	$cm^3\ cm^{-3}$	Dai et al. (2013)
	Residual soil moisture		[0.000, 0.100]	$cm^3\ cm^{-3}$	Dai et al. (2013)
	Saturated hydraulic		[5.7, 266.	$cm\ d^{-1}$	Dai et al. (2013)

Type	Parameter	Original resolution	Value range	Unit	Source
	conductivity		2]		
	The inverse of air-entry value (α) in the van Genuchten Functions		[0.008, 0.042]	cm^{-1}	Dai et al. (2013)
	The shape parameter (n) in the van Genuchten Functions		[1.114, 1.524]	–	Dai et al. (2013)
	Soil layer depth		[1.8, 2.5]	m	FAO et al. (2009)
	Soil clay content		[5, 54]	% wt.	FAO et al. (2009)
	Soil sand content		[12, 89]	% wt.	FAO et al. (2009)
	Soil organic carbon content		[0.41, 33.54]	% wt.	FAO et al. (2009)
Land use and	Land use map	One-time and 30 m × 30 m	–	–	Cold and Arid Regions Science Data

Type	Parameter	Original resolution	Value range	Unit	Source
					Center (http://westdc.westgis.ac.cn)
vegetation data	Digital elevation model (DEM)	One-time and 90 m × 90 m	[2656, 6252]	m	Jarvis et al. (2008)
	Leaf area index (LAI)	15-day and 0.0833° × 0.0833°	–	–	Zhu et al. (2013)
	Fraction of photosynthetically active radiation (FPAR)	15-day and 0.0833° × 0.0833°	–	–	Zhu et al. (2013)
Validation data	River discharge	Daily at 3 stations	–	$m^3\ s^{-1}$	Annual Hydrological Report by the Ministry of Water Resources of China
	Soil temperature (from 5 cm to 320 cm depth)	Daily at 11 stations	–	°C	China Meteorological Administration (http://data.cma.cn)
	Map of	One-time and	–	–	Li and Cheng (1996)

Type	Parameter	Original resolution	Value range	Unit	Source
	Permafrost on the Qinghai-Tibet Plateau (MP-QTP)	scale 1:3,000,000			

The climatic forcing data include daily precipitation, daily air temperature (mean, maxima and minima), daily average wind speed, daily average relative humidity and daily sunshine duration. These data were observed at 22 meteorological stations managed by the China Meteorological Administration (CMA) within or around the study area. The observations were fully quality controlled and downloaded from the National Meteorological Information Center (NMIC) of the CMA (http://data.cma.cn). Gridded precipitation with a 3-km resolution was spatially interpolated from gauge observations using the climatology-based optimal method proposed by Shen and Xiong (2016). Other climatic data were spatially interpolated using an angular distance weighting method with elevation corrections (Yang et al., 2004). The spatial resolution of the gridded climatic forcing dataset was 3 km × 3 km. Hourly air temperature was estimated using the daily mean, maxima and minima and a sine curve (Gao et al., 2016). Hourly precipitation was estimated from the daily precipitation data according to the precipitation duration, which was estimated by the amount of precipitation from historical records. The starting hour of precipitation was randomly selected, and the hourly precipitation was then specified following a normal distribution. Details on the algorithm can be found in Gao et al. (2016).

Soil water parameters, including saturated soil moisture, residual soil moisture and soil hydraulic conductivity, were obtained from the China Soil Hydraulic Parameters Dataset (Dai et al., 2013). The soil map of the study area was obtained from the Harmonized World Soil Database (HWSD) produced by the Food and Agriculture Organization of the United Nations (FAO et al., 2009). The land use map was obtained from Cold and Arid Regions Science Data Center at Lanzhou (CARD) (http://westdc.westgis.ac.cn). This study used the shuttle radar topography mission (SRTM) digital elevation model (DEM) with a resolution of 90 m (Jarvis et al., 2008). The vegetation parameters in the model include the leaf area index(LAI) and the fraction of photosynthetically active radiation (FPAR). This study used the LAI3g and FPAR3g datasets (Zhu et al., 2013), which were derived from the 3rd generation of Normalized Difference Vegetation Index (NDVI3g) of the Global Inventory Modeling and Mapping Studies (GIMMS). The NDVI3g, LAI3g and FPAR3g datasets have been well evaluated in previous studies and exhibited satisfactory performance in capturing

the vegetation dynamics on the Qinghai-Tibet Plateau (Che et al., 2014, Cong et al., 2016, Gao et al., 2016).

Daily river discharge data are available from Tangnaihai (TNH) and Maqu (MAQ) hydrological stations for the period 1981–2015. At Jimai (JMA) station, daily discharge data are available from 2001 to 2015 and monthly data are available during 1981–2000. The river discharge data were obtained from the Annual Hydrological Report published by the Ministry of Water Resources of China. Permafrost and seasonally frozen ground observations were collected at eleven CMA meteorological stations in the study area. According to the CMA (2007), the daily frozen depth is manually measured by the standard frozen soil apparatus. The apparatus is vertically buried in the meteorological field, and the frozen depth is measured by the length of ice in the inner rubber tube. The temporal ranges of available datasets vary at different stations, although most stations have continuous soil temperaturedata during 2004–2015 and continuous frozen ground depth data during 1981–2015. The datasets of soil temperature and frozen ground depth were obtained from the NMIC of the CMA (http://data.cma.cn). Additionally, soil temperature profiles measured in four 20-m boreholes on October 13, 2011 were obtained from Luo et al. (2012), and the locations of these boreholes are shown in Fig. 1. The “Map of Permafrost on the Qinghai-Tibet Plateau” (MP-QTP) (Li and Cheng, 1996) and its digital files were downloaded from the CARD.

3. Model description

3.1. Overall model structure and function

In this study, a geomorphology-based eco-hydrological model (GBEHM) (Gao et al., 2016) is applied to the Yellow River source region. GBEHM is a distributed hydrological model that was primarily developed to simulate hydrological processes by considering the soil freezing and thawing processes in cold regions. GBEHM originates from a geomorphology-based hydrological model (GBHM) (Yang et al., 1998, Yang et al., 2002). The major improvements of GBEHM over GBHM are as follows: (i) the distributed scheme for eco-hydrological modeling was improved (Yang et al., 2015); (ii) the simple biosphere model (SiB2) was used for evapotranspiration (ET) estimation (Gao et al., 2016); and (iii) a new energy balance module was added for simulating soil freezing-thawing changes, snow ice/water phase

changes and hydrological processes in cold regions (Gao et al., 2016, Gao et al., 2017a).

The overall structure of the GBEHM from top to bottom includes the study basin, sub-catchments, flow intervals, grid cells, and hillslopes in each grid cell (see Fig. S1 in the supplementary material). A topographically similar hillslope-valley system (lower right panel in Fig. S1) is used for sub-grid parameterization; therefore, hillslope is the computational unit used for eco-hydrological simulations in the GBEHM (Yang et al., 2002, Yang et al., 2015). The hillslope is parameterized by the slope length (l) and slope angle (β), and the water heads (h and H) are used to simulate the infiltration and water flow in the subsurface (Yang et al., 2015). In the present study, a grid system with a 3-km resolution is used to discretize the study area, and each grid cell is characterized by a number of topographically similar hillslopes. The meander ratio is used to correct the river length extracted from the 3-km DEM, which is estimated as the ratio of the total river length extracted from the original 90-km DEM to that from the 3-km DEM (1.14 for the study area). Additional details on the model structure and physical representations of the landscape can be found in recent studies by Yang et al. (2015), Li et al. (2015b), Gao et al. (2016), Miao et al. (2016) and Gao et al. (2017a). This paper briefly introduces the soil freezing-thawing processes, evapotranspiration, and runoff generation in the GBEHM in the following sections.

3.2. Soil freezing and thawing

The soil freezing and thawing processes are represented by a coupled heat and water balance equation. The energy balance equation is expressed as (Flerchinger and Saxton, 1989)

$$\rho_{ice} L_f \frac{\partial \theta_{ice}}{\partial t} - C_s \frac{\partial T}{\partial t} + \frac{\partial}{\partial z}\left(k_s \frac{\partial T}{\partial z}\right) + \rho_{liq} C_{liq} \frac{\partial q_{liq} T}{\partial z} = 0, \qquad (1)$$

where ρ_{ice} and ρ_{liq} are the ice density and liquid water density (kg m^{-3}), respectively; L_f is the latent heat of fusion (3.34×10^5 J kg^{-1}); θ_{ice} is the ice content of the frozen soil(m^3 m^{-3}); t is the time step (s); C_s is the volumetric heat capacity of the frozen soil (J m^{-3} K^{-1}); C_{liq} is the gravimetric heat capacity of liquid water (J kg^{-1} K^{-1}); q_{liq} is the liquid water flux between soil layers and is determined using the Richards' equation; k_s is the thermal conductivity of the soil (W m^{-1} K^{-1}), which is estimated

according to Johansen's scheme (Johansen, 1975, Farouki, 1981); T is the soil temperature; and z is the soil depth (m).
The unsaturated soil hydraulic conductivity is estimated using a variant of the van Genuchten Function as in Wang et al. (2010)

$$K = f_{ice} K_{sat} \left(\frac{\theta_{liq}-\theta_r}{\theta_s-\theta_r}\right)^{1/2} \left[1-\left(1-\left(\frac{\theta_{liq}-\theta_r}{\theta_s-\theta_r}\right)^{-n/(n-1)}\right)^{(n-1)/n}\right]^2 \quad (2)$$

where K and K_{sat} are the unsaturated and saturated soil hydraulic conductivity (m s^{-1}), respectively; θ_{liq} is the liquid water content of the frozen soil (m^3 m^{-3}); θ_s and θ_r are the saturated soil moisture and residual soil moisture (cm^3 cm^{-3}), respectively; and n is the shape parameter of the van Genuchten Function. Additionally, f_{ice} is the reduction factor of hydraulic conductivity, or the “impedance factor” (Stähli et al., 1996), and it is calculated based on the soil temperature T

$$f_{ice} = \exp(-10 \cdot (T_f - T)) \text{ and } 0.05 \le f_{ice} \le 1.00 \quad (3)$$

where T_f is the freezing point of water (273.15 K). It should be noted that the impedancefactor approach for the unsaturated frozen soil is not ideal and could cause unstable simulations at temperatures close to the T_f (Kurylyk and Watanabe, 2013). Considering the computational costs associated with large-scale simulations, we use this simple method to estimate the reduction in hydraulic conductivity.
The topsoil layer receives a heat flux from the atmosphere and is used to establish the upper boundary condition for the layer below [see Eq. (1)]. The heat flux from the atmosphere into the topsoil layer is calculated as (Oleson et al., 2010)

$$h = R_n - H - \lambda E + Q_r \quad (4)$$

where h is the heat flux from the atmosphere into the topsoil layer (W m^{-2}); R_n is the net radiation from the atmosphere into the topsoil layer (W m^{-2}); H and λE are the sensible and latent heat fluxes from the topsoil into the atmosphere (W m^{-2}); and Q_r is the heat flux associated with rainfall (W m^{-2}).
The lower boundary condition for soil heat transfer is assumed to be the zero-heat flux boundary at the depth of 50 m. Because geothermal heat flux data are not available in the study area and the average thickness of seasonally frozen ground is less than that of permafrost, the zero heat flux

and 50-m soil layer are considered proper boundary conditions, which will be validated using soil temperature data from borehole observations in the following validation section.

3.3. Evapotranspiration

The evapotranspiration from vegetation canopy and evaporation rate from soil are simulated in the GBEHM (Gao et al., 2016). The transpiration rate of the canopy layer E_{ct} is calculated using the same algorithm as given in the SiB2 model, which is expressed as (Sellers et al., 1996)

$$\lambda E_{ct} = \left[\frac{e^*(T_c) - e_a}{1/g_c + 2r_b}\right]\frac{\rho_a c_p}{\gamma}(1 - W_c) \quad (5)$$

where λ is the latent heat of vaporization (J kg^{-1}); E_{ct} is the canopy transpiration rate (kg m^{-2} s^{-1}); $e^*(T_c)$ is the saturated vapor pressure (Pa) at the canopy temperature T_c (K); $e_{a.}$ is the canopy air space vapor pressure (Pa); g_c is the canopy conductance (m s^{-1}); r_b is the canopy boundary layer resistance (s m^{-1}); ρ_a is the density of air (kg m^{-3}); c_p is the specific heat of air (J kg^{-1} K^{-1}); γ is the psychrometric constant (Pa K^{-1}); and W_c is the fractional wetted area of the canopy. The value of the canopy conductance g_c is estimated as (Sellers et al., 1996)

$$g_c = m\frac{A_c}{C_s}h_s p_a + bL_T \quad (6)$$

where m and b are the empirical coefficients for C_3 or C_4 vegetation (m s^{-1}); C_s is the CO_2partial pressure at leaf surface (Pa); h_s is the relative humidity at leaf surface; p_a is the atmospheric pressure (Pa); L_T is the total LAI of the canopy (m^2 m^{-2}); and A_c is the canopy photosynthesis rate (mol m^{-2} s^{-1}), which is calculated as (Sellers et al., 1996)

$$A_c = A_{n0}\Pi \quad (7)$$

$$\Pi \approx \mathrm{FPAR}/\bar{k} \quad (8)$$

where A_{n0} is the net assimilation rate A_n for leaves at the top of the canopy (mol m^{-2} s^{-1}); FPAR is the fraction of photosynthetically active radiation absorbed by the canopy; and k^- is the mean canopy extinction coefficient. The net assimilation rate A_n (mol m^{-2} s^{-1}) is estimated as (Sellers et al., 1996)

$$A_n = A_l - R_d \quad (9)$$

where A_l is the leaf photosynthetic rate (mol m^{-2} s^{-1}); and $R_{d.}$ is the leaf respiration rate (mol m^{-2} s^{-1}). A_l and $R_{d.}$ are estimated by the parameter V_{max} (the maximum catalytic capacity of the

photosynthetic enzyme, RuBisCO), canopy temperature, soil moisture stress, and other environmental factors. Details can be found in Sellers et al. (1996). The evaporation rate of the canopy interception E_i and the evaporation rate of the surface soil layer E_g are calculated by the same algorithm as in the SiB2 (Sellers et al., 1996). E_{ct}, E_i, and E_g are added as the total actual evapotranspiration from the land surface of the hillslope. Detailed equations on the canopy energy transfer and the photosynthetic processes in the GBEHM can be found in Gao et al. (2016).

3.4. Runoff generation

By solving the Richards' equation, the surface runoff from the infiltration excess and/or saturation excess can be calculated. The groundwater runoff discharging into the river is considered as steady flow and is calculated using Darcy's law (Yang et al., 2002). Runoff generated from each grid cell is the lateral inflow into the river channel. Flow routing in the river channel is calculated using the kinematic wave approach as

$$\begin{cases} q = \frac{\partial A}{\partial t} + \frac{\partial Q}{\partial x} \\ Q = \frac{S_0^{1/2}}{n_r \cdot p^{2/3}} A^{5/3} \end{cases} \quad (10)$$

where q is the lateral inflow per unit length ($m^2\ s^{-1}$); A is the area of the river channel cross-section (m^2); t is the time step (s), which is set as 1 h in this simulation; x is the distance along the stream; Q is the river discharge ($m^3\ s^{-1}$); S_0 and n_r are the slope and roughnessof the riverbed, respectively; and p is the wetted perimeter of the channel cross-section (m).

3.5. Model setup and calibration

The initial variables in GBEHM include the soil moisture, soil temperature groundwater table, etc. In this study, we used a 10-year warm-up run to spin up the GBEHM and initialize the hydrological conditions in the study area (Li et al., 2015b). The daily river discharge data during 1981–1990 at TNH station were used to calibrate the model parameters. The manually calibrated parameters in the GBEHM included the saturated hydraulic conductivity of the topsoil, groundwater hydraulic conductivity and slope shape factor. After calibration, we used the river discharge data from 1991 to 2000 for model validation, and simulations were then performed from 2001 to 2015. Simulations for the entire study period from 1981 to 2015 were

driven by the gridded climatic forcing dataset with a temporal resolution of 1 h.

4. Results

4.1. Model validation

The observed and simulated daily river discharge at TNH station during 1981–1990 (calibration period) and during 1991–2000 (validation period) are shown in Fig. 2. The evaluation metrics of streamflow simulations at three hydrological stations are listed in Table S1 in the supplementary material. The Nash-Sutcliffe efficiency (NSE), coefficient of determination (R^2), root-mean-square error (RMSE), and percent bias (PBIAS) were used to measure the model performance (Moriasi et al., 2007). The simulated river discharge at TNH station, which is located at the outlet of the entire study basin, was generally consistent with the observations. The NSE, R^2, RMSE and PBIAS for the calibration period were 0.77, 0.84, 335.9 $m^3 s^{-1}$ and 1%, respectively. The model simulation exhibited a similar performance during the validation period, and the NSE, R^2, RMSE and PBIAS values were 0.67, 0.73, 250.3 $m^3 s^{-1}$ and 2%, which indicate that the simulations at the basin scale were satisfactory (Moriasi et al., 2007). The simulated river discharge at MAQ station exhibited similar performance to that at TNH station as reflected by the evaluation metrics in Table S1. At JMA station, the statistics were slightly worse because parameters were not specifically calibrated for smaller sub-basins. However, the model captured the temporal variability in streamflow at JMA station reasonably well, and the R^2 exceeded 0.70 and NSE was greater than 0.50. The overestimations of the descending limbs of the hydrographs as shown in Fig. 2 were potentially caused by errors in the soil depth map, which will be discussed in the Discussion section.

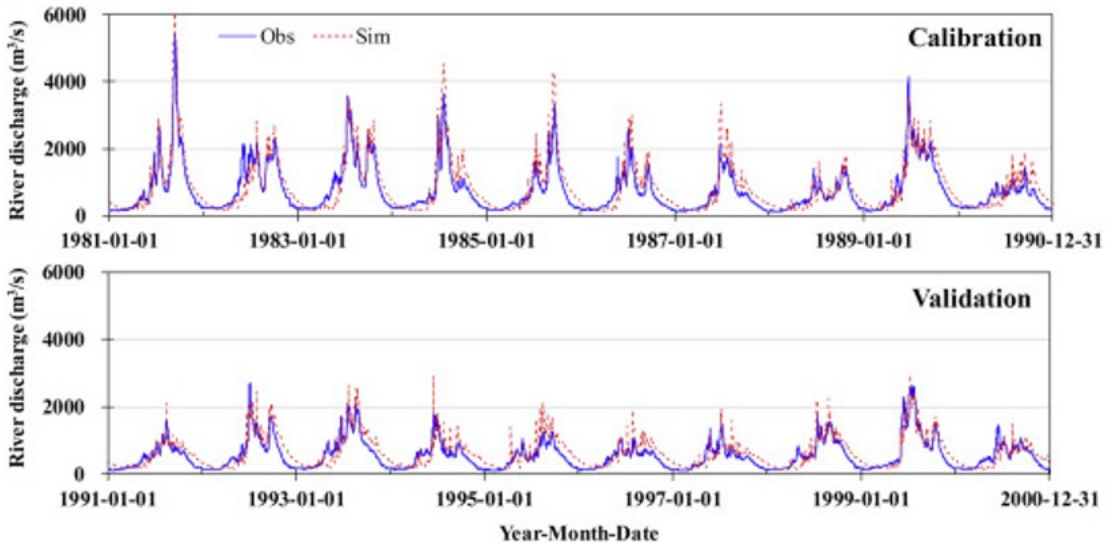

Fig. 2. Comparisons of simulated (Sim) and observed (Obs) daily streamflow at Tangnaihai (TNH) station during the calibration period of 1981–1990 and validation period of 1991–2000. The Nash-Sutcliffe efficiency (NSE), coefficient of determination (R^2) and mean percent bias (PBIAS) are listed in Table S1 in the supplementary material.

The frozen ground depth was validated using site observations. Fig. 3 shows that, the simulated frozen ground depth of the model is significantly correlated with the observations (R^2 = 0.61 and *p*-value < 0.05), and the deviations are within an acceptable range (RMSE = 0.37 m and PBIAS = 5%). Additionally, the model simulation generally captured the seasonal variations in the observed frozen ground depth. Deficiencies in the GBEHM simulations include overestimations of the frozen ground depths at elevations of 3000–3600 m and underestimations at elevations of 3600–4200 m a.s.l. These inaccuracies may be related to errors in the climatic forcing data, which are spatially interpolated from the eleven meteorological stations, and seven of these stations are located at moderate elevations from 3400 m to 3800 m.

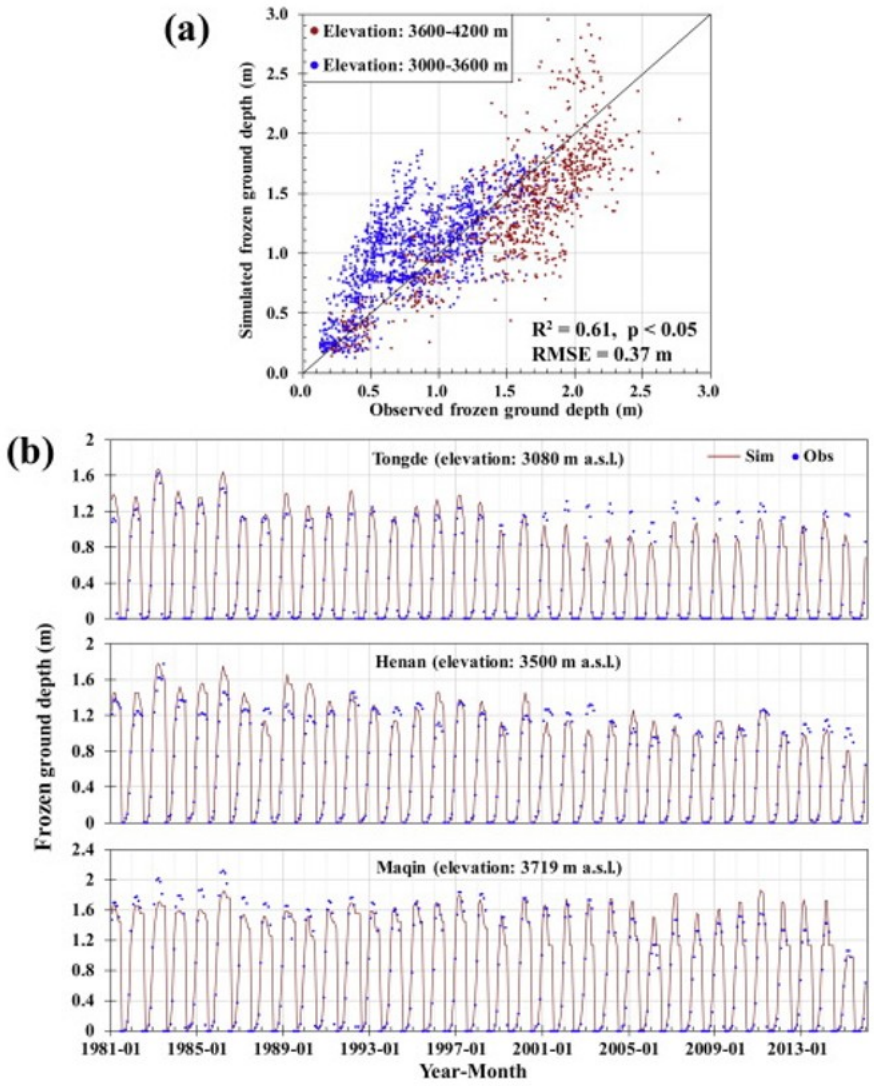

Fig. 3. (a) Comparisons of the simulated and observed frozen ground depths at eleven meteorological stations in the study area and (b) monthly variations in the simulated (Sim) and observed (Obs) frozen ground depths at Tongde, Henan and Maqin stations during 1981–2015.

Comparisons of the simulated and observed 20-m soil temperature curves at four boreholesare provided in Fig. S2 in the supplementary material. In general, the simulation captured the vertical variations in the soil temperature from 0 m to 20 m, with R^2 values ranging from 0.84 to 0.96 and RMSE values ranging from 0.36 °C to 0.65 °C; however, the temperature values were overestimated above 5 m at CLP-3 and CLP-4. These discrepancies of soil temperature near the ground surface could have been caused by the climatic data, which were spatially interpolated from in situ meteorological observations, and the interpolation may not be accurate at

the two high-elevation boreholes (4663 m and 4564 m a.s.l.). In addition, the heterogeneity of soil properties, especially the soil thermal conductivity and heat capacity, may introduce estimation errors.
Long-term soil temperature profiles at three CMA meteorological stations are shown in Fig. S3 in the supplementary material. In addition to the zero-degree isotherm, which was treated as the frozen ground depth, Fig. S3 illustrates that the simulated soil temperature profiles are in good agreement with observed temperature profiles. Therefore, the performance of GBEHM is generally satisfactory for analyzing frozen ground changes in the study area.

4.2. Spatio-temporal variations in the frozen ground

Fig. 4 presents a comparison of the simulated spatial distributions of permafrost and seasonally frozen ground over the past three decades with those from MP-QTP (Li and Cheng, 1996). In this study, a grid was characterized as permafrost when the frozen ground depth was greater than zero year-round. The estimated decadal permafrost distribution in this study is generally consistent with that of the MP-QTP, which was mapped based on in situ investigations from 1983 to 1995 (Ran et al., 2012). At the decadal scale, the distribution of permafrost shrunk from the 1980s to the 2000s in the central and northwestern parts of the study area. Additionally, the areas of permafrost in the study period are listed in Table S2 in the supplementary material. The area of permafrost was 54,171 km^2 during 1981–1990, and it decreased to 20,916 km^2 during 2001–2010. As shown in Fig. S4 in the supplementary material, the areal mean maximum thickness of seasonally frozen ground (MTSFG) ranged from 1.1 m to 1.8 m in the Yellow River source region. The MTSFG decreased by 0.012 m per year during 1981–2015, and the trend was statistically significant at a level of 0.05. In addition, the permafrost area ratio in the study area decreased by 1.1% per year over the past 35 years. Moreover, the MTSFG and permafrost areas decreased sharply after year 2000, and these trends were consistent with the notable temperature increase.

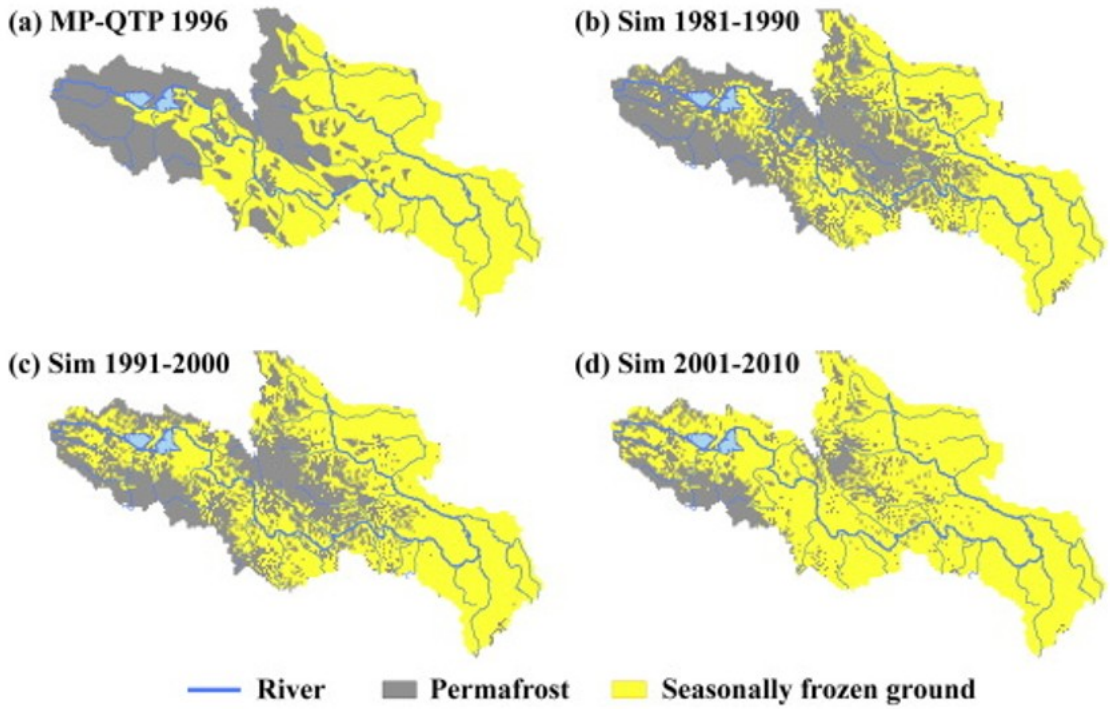

Fig. 4. Spatial distributions of permafrost and seasonally frozen ground from (a) the “Map of Permafrost on the Qinghai-Tibet Plateau” (MP-QTP) (Li and Cheng, 1996) and from the simulated (Sim) permafrost map of this study in the Yellow River source region during (b) 1981–1990, (c) 1991–2000 and (d) 2001–2010. The areas of permafrost and seasonally frozen ground in each map are listed in Table S2 in the supplementary material.

4.3. Spatial patterns and temporal trends of the water balance components

Fig. S5 in the supplementary material shows the spatial distributions of the annual mean precipitation, ET, and runoff as well as the average soil moisture of the top 50 cm of the soil in the growing season (i.e., from May to October) during 1981–2015. The annual mean precipitation exhibited a spatial pattern similar to that of the runoff, which implies that runoff is mainly generated from precipitation in the growing season. Moreover, the spatial pattern of the actual ET was consistent with that of soil moisture because of the water supply from soil. The annual precipitation ranged from 300 mm to 900 mm, with a mean value of 547 mm. The lowest annual precipitation was observed in the northwestern part of the Yellow River source region, and precipitation generally increased from northwest to southeast along with decreasing elevation. The highest values of ET and soil moisture were observed in the southeastern part. The areal mean ET and

runoff were 372 mm and 175 mm, which indicated that 68% of the rainfall evaporated in this arid and cold region.

The inter-annual variations in the water balance components and mean air temperature are shown in Fig. 5. The variations in annual runoff were highly consistent with those of precipitation, with a coefficient of determination of 0.85. This finding implies that the inter-annual variations of runoff is mainly controlled by precipitation in the study area. The annual precipitation decreased significantly at a level of 0.05 from 1981 to 2002, which represented a decreasing rate of 58.4 mm/10 a and a net decrease of 122.6 mm. Since 2002, the annual precipitation has increased by 71.1 mm/10 a. The mean air temperature significantly increased by 0.66 °C/10 a, or a net change of 2.2 °C, during the study period, and it increased more sharply from 1995 to 2015 (0.75 °C/10 a). Accordingly, the annual ET increased significantly by 14.3 mm/10 a. The temporal variations in ET were consistent with the mean air temperature, and the coefficient of determination was 0.59, which is because of the enhanced vegetation activity in a warming environment given in the model setting (see Section 3.3). These results imply that the climate of the Yellow River source region became progressively warmer and wetter during the study period.

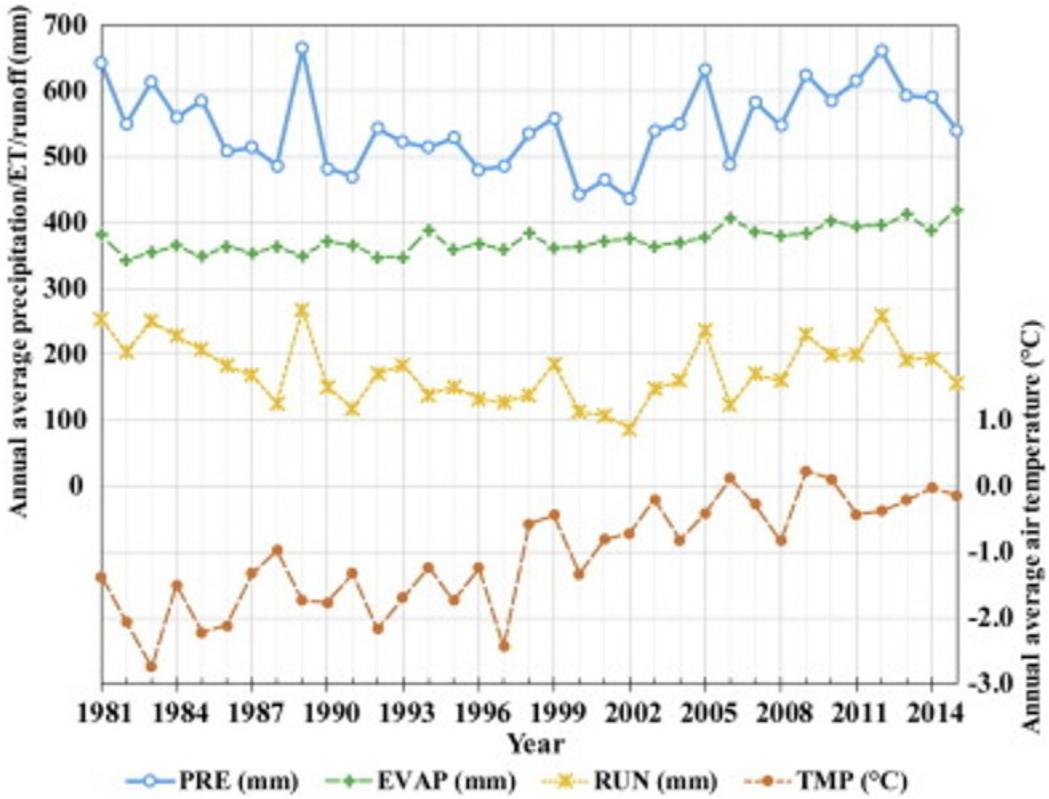

Fig. 5. Inter-annual variations in annual average precipitation (PRE), evapotranspiration (EVAP), runoff (RUN), and air temperature (TMP) in the Yellow River source region during 1981–2015.

4.4. Changes in the river flow regime

Decadal variations in the hydrographs are provided in Fig. 6. We listed the mean daily river discharge for the periods 1981–1990, 1991–2000 and 2001–2010 at three hydrological stations (i.e., TNH, MAQ and JMA) and the total runoff from the sub-catchments in the permafrost region. The average river discharge at the decadal scale is employed to analyze the long-term changes in flow regime and discuss the impacts of climate change. In addition, the day-of-year (DOY) values of the 25%, 50% and 75% breakpoints (D25, D50 and D75) of inter-annual mean river discharge are listed in Table S3 in the supplementary material. The highest river discharge was observed during 1981–1990 because of the high precipitation in this period. For the annual streamflow of the entire study area, the D25 values of hydrographs at TNH occurred ten days earlier in the 1980s compared to those in the 1990s. This result implies that although the annual river discharge decreased in the 1990s, the runoff contributions to annual river runoff increased in the early months of the year.

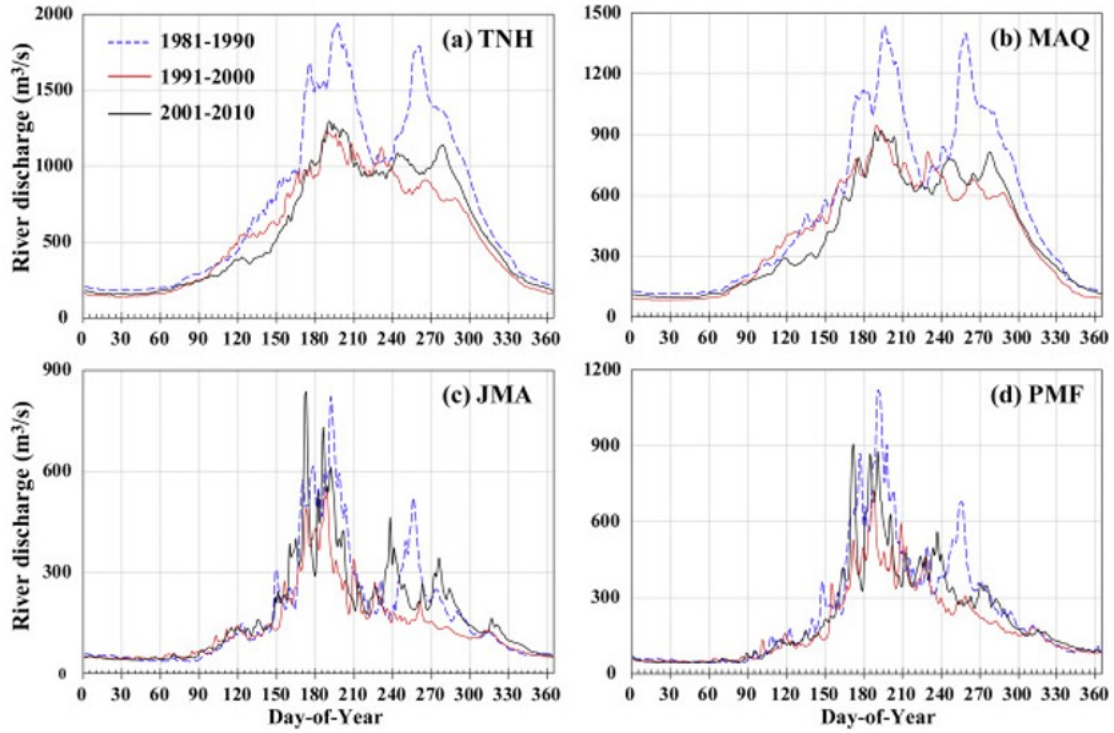

Fig. 6. Daily hydrographs of mean river discharge in the periods of 1981–1990, 1991–2000 and 2001–2010 at (a) Tangnaihai (TNH), (b) Maqu (MAQ), (c) Jimai (JMA) stations and in (d) the permafrost region (PMF).

The results show that the D25 values of hydrographs at JMA were close to those at TNH in each decade (159th to 171th DOY), but D50 and D75 at JMA were observed 12–20 days earlier than those at TNH. The runoff from the sub-catchments in the permafrost region exhibited a hydrograph similar to that observed at JMA station (see Fig. 6). However, the runoff coefficients (i.e., annual runoff divided by annual precipitation) generally decreased in the past three decades because of the increase in ET (see Table S3 in the supplementary material). The rising air temperature, thawing permafrost and increasing precipitation combined to increase runoff at JMA and in the permafrost sub-catchments.

4.5. Changes in vegetation growth

Fig. 7 compares the spatial distributions of the trends of LAI, simulated ET, frozen ground depth and soil moisture in the upper 50-cm soil layer to analyze the vegetation response to climate change and frozen soil degradation during 1982–2011. To focus on the impact of frozen soil, the annual change rates were calculated at the start of the vegetation growing

season (from March to May) for each index. Because the LAI data are available only from July 1981 to December 2011, the time periods have been unified as 1982–2011 to make the change rates of variables comparable. The remote sensing-based data show that LAI significantly increased in most parts of the study area, although it significantly decreased in the northeast. Notably, the areal mean LAI increased by 2.1×10^{-3} per year in 46.7% of the study region. The change rates of ET were consistent with those of the LAI. The frozen ground depth at the start of the growing season significantly decreased in this region, and the largest decreasing rates were simulated in the central and northeastern parts of the region. The topsoil moisture at the start of the vegetation growing season exhibited an increasing trend in most of the study area but a significantly decreasing trend in the northeast.

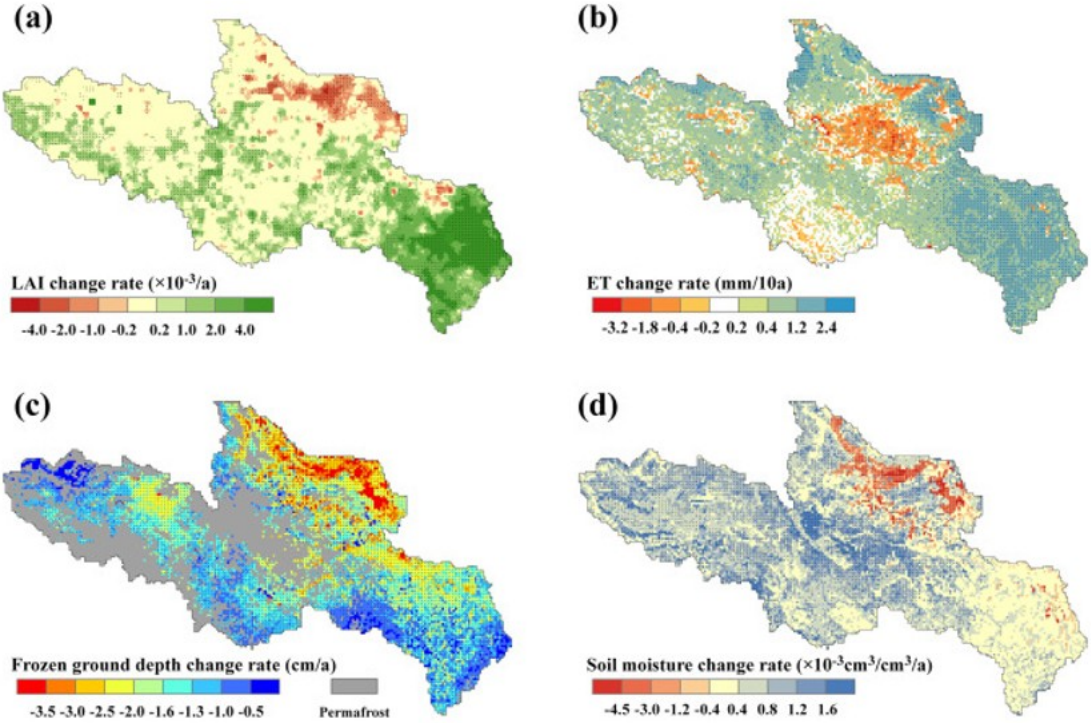

Fig. 7. Spatial distributions of the change rates of (a) the leaf area index (LAI), (b) evapotranspiration(ET), (c) the seasonally frozen ground depth, and (d) the liquid soil moisture in the top 50-cm soil layer. All the change rates were calculated from March to May in 1982–2011. Dots in the figure represent significant trends at a level of 0.05.

Based on the spatial distributions of the change rates as shown in Fig. 7, we analyze the correlations among the trends of the LAI, ET, soil moisture, and frozen ground depth. The results show that the increase of ET is associated with the significant increase of LAI (Fig. S6a in the supplementary material).

The changes of frozen ground depth exhibit complex relationships with changes of the LAI and soil moisture (Fig. S6b and d). The modest decreases of the frozen ground depth (from 0 to − 3 cm/a) have a slight positive effect on the soil moisture (from 0 to 2×10^{-3} $cm^3/cm^3/a$) but a considerable positive impact on the LAI because of the synchronous increase of temperature. However, the greatest decreases of the frozen ground depth (<− 3 cm/a) are likely to decrease the soil moisture and result in a decrease of LAI (from 0 to -4×10^{-3}/a). The modest increase in temperature, decrease in frozen ground depth and increase in root-zone soil moisture generally had positive effects on vegetation growth, which is reflected by the increasing LAI. The northeastern portion of the study area received relatively little precipitation (< 400 mm) as shown in Fig. S5. The rapid decrease in the frozen ground depth caused soil moisture to decrease and could be the reason for the abnormal decrease in the LAI.

Furthermore, we divided the study area into three zones to analyze the impacts of frozen ground changes on vegetation growth. Considering the decadal changes from permafrost to seasonally frozen ground as shown in Fig. 4, the three zones are defined as the permafrost area in the 2000s (see Fig. 4b), seasonally frozen ground in the 1980s (see Fig. 4d) and the transition zone from permafrost to seasonally frozen ground during 1980–2010. To clarify the differences in vegetation responses, Table S4 in the supplementary material lists the means and trends of LAI, ET and topsoil moisture from March to May during the study period in the three zones. Seasonally frozen ground exhibited the largest mean LAI (0.308), ET (28.3 mm) and topsoil moisture (0.352 cm^3/cm^3). The LAI and ET significantly increased by 1.15×10^{-3}/a and 0.07 mm/a, respectively. Additionally, the areal average LAI of the permafrost zone increased significantly by 0.71×10^{-3}/a because of the significant increases in topsoil moisture and temperature. The transition zone from permafrost to seasonally frozen ground exhibited the greatest increase in topsoil moisture (0.94×10^{-3} $cm^3/cm^3/a$), which may have led to further increases in the LAI and ET.

5. Discussion

5.1. Impacts of frozen ground changes on eco-hydrology

The frozen ground changes in the Yellow River source region were highlighted in this study. The results show that the permafrost area and the

frozen ground depth decreased during the study period. Previous studies indicated that melt water runoff increased, but its contribution to annual streamflow was negligible in this region (Cuo et al., 2013). This study also shows that frozen ground changes further increased the river discharge during the cold season, as reflected by the daily hydrographs (see Fig. 6). This result could be explained by a shift in aquifer permeability, enhanced surface water infiltration and increased subsurface flow (Bense et al., 2012, Cheng and Jin, 2013, Gao et al., 2017b). This finding agrees with the results of studies in Northwest China, which showed that accelerated frozen ground degradation was the main driving factor of increased baseflow (Qin et al., 2016). Moreover, most previous models were based on the assumption that land cover and land use changeswere independent of climate change (Zheng et al., 2009, Cuo et al., 2013), but they neglected the potential effects of permafrost degradation on land cover changes due to climate change. Therefore, our study complements previous hypotheses of the relationship between hydrology and frozen ground changes.

Several previous studies investigated the effects of permafrost and seasonally frozen ground degradation on vegetation growth (Jin et al., 2009, Dorji et al., 2013, Cable et al., 2014, Iijima et al., 2014). However, there were many discrepancies in the different studies. Thus, it remains unclear whether permafrost and seasonally frozen ground degradation has positive effects (Cuo et al., 2015, Qin et al., 2016) or negative effects (Jin et al., 2009, Iijima et al., 2014) on vegetation growth. In this study, we employed a process-based model to analyze frozen ground degradation and provided quantitative explanations based on numerical simulations. Previous studies indicated that frozen ground changes mainly affected vegetation growth at the start of the growing season on the Qinghai-Tibet Plateau (Zhang et al., 2015, Qin et al., 2016). Our results further suggest that soil moisture increased with a modest decrease in the frozen ground depth (>-3.0 cm/a), which caused increases in the LAI and ET at the start of the growing season. Additionally, discrepancies in the vegetation responses to frozen ground degradation were observed. The northeastern portion of the study region exhibited the greatest decreases in the frozen ground depth (<-3.0 cm/a) and LAI ($< -1.0 \times 10^{-3}$/a). These spatial variations are potentially due to different soil types and the lowering groundwater table

(Cheng and Wu, 2007). Therefore, we argue that the rate of change of the frozen ground depth is an important factor in analyses of the vegetation response to permafrost degradation.

5.2. Comparison with previous studies

We investigated the recent changes in the water balance components and frozen ground on the northeastern Qinghai-Tibet Plateau over the past 35 years (1981–2015). The distribution of permafrost and seasonally frozen ground was consistent with the results presented in a previous study (Li and Cheng, 1996), and the mean change rate of the frozen ground depth (− 1.2 cm/a) was greater than that of previous results (− 0.40 cm/a and − 0.74 cm/a) in regions of seasonally frozen ground on the Qinghai-Tibet Plateau (Wang et al., 2015, Qin et al., 2016). This change rate of frozen ground depth was also greater than the average rate in China, which was estimated as − 0.18 cm/a based on data collected at observation stations (Peng et al., 2017). This study estimated that the permafrost area in the Yellow River source region decreased by 1.1% per year. This rate is greater than a previous estimate across China, which suggested that the permafrost area decreased by 18.6% from the 1970s to the 2000s (Cheng and Jin, 2013). The above results distinguish the present study region from previous investigations. Because the Yellow River source region is located in a transition zone between permafrost and seasonally frozen ground, the change rates of the permafrost area ratio and frozen ground depth could be greater than the average rates on the Qinghai-Tibet Plateau or in China. Therefore, our study on the northeastern margin of the Qinghai-Tibet Plateau provides a regional-scale result of accelerated frozen ground degradation in recent years.

Our results showed that vegetation responses to frozen ground degradation vary spatially with the change rate of the frozen ground depth, which may explain the discrepancies of recent studies in cold regions (Dorji et al., 2013, Cable et al., 2014, Iijima et al., 2014, Zhang et al., 2015). In permafrost regions in Alaska (Cable et al., 2014) and eastern Siberia (Iijima et al., 2014), the significant warming and thawing of permafrost caused waterlogged soil conditions and restrained the growth of trees. In arid and cold regions, such as the Qinghai-Tibet Plateau, the degraded frozen ground and wet climate enhanced the growth of shallow-rooted meadows (Zhang et

al., 2015), which was partially related to the increase in upper soil moisture (Dorji et al., 2013). However, our model simulations further demonstrated that if the frozen ground depth decreases too fast, the soil moisture could decrease, which would negatively affect the vegetation growth. This finding is consistent with in situ investigations showing that fast permafrost degradation could lower the groundwater table and restrain vegetation growth (Jin et al., 2009, Cheng and Jin, 2013).

5.3. Uncertainties and limitations

There are uncertainties associated with the model simulations. The present study used the HWSD dataset (FAO et al., 2009) to estimate the soil layer depth; therefore, uncertainties may have occurred in the soil depth because of this global dataset. The soil depth is characterized by the soil types in the HWSD; thus, the inhomogeneity among soil types may not be fully captured at the regional scale. Additionally, soil parameters can also affect the hydrological simulations in the present model [details can be found in Li et al. (2012)], which may explain the errors of the descending limbs in the hydrographs as shown in Fig. 2 and Section 4.1.
As shown in Fig. 1, Fig. 4, the meteorological stations are located on seasonally frozen ground, so the validation of the frozen ground depth, as shown in Fig. 3, mainly represented the changes in the seasonally frozen ground. In this study, inter-annual variations in vegetation growth were represented by the remote sensing-based LAI. The vegetation responses to frozen ground changes could be diverse according to vegetation types and root depths. This study assumed that vegetation type was not a decisive factor regarding the vegetation response to frozen ground changes. These assumptions were considered valid because the dominant vegetation types are shallow-rooted alpine meadows and steppes(Jin et al., 2009, Zhang et al., 2009), and their spatial and temporal changes can be well evaluated using remote sensing data (Li et al., 2015a).

6. Conclusion

This study performed a 35-year simulation (1981–2015) of the eco-hydrological processes, including the freezing and thawing of the soil, in the Yellow River source region. The spatio-temporal characteristics of the changes in water balance components and frozen groundwere analyzed, and

the impacts of climate change on streamflow and vegetation growthwere discussed. According to the results of this study, the following conclusions were drawn.

(1) With the parameterization of the soil freezing and thawing processes, the eco-hydrological model (i.e., GBEHM) used in this study reasonably reproduced the historical trends and inter-annual variations in river discharge, frozen ground depth and soil temperature profile.

(2) The frozen ground depth exhibited a significant decreasing trend, and the areal mean frozen ground depth decreased by 0.012 m per year during 1981–2015. Additionally, the areal ratio of permafrost decreased by 1.1% per year in the study region.

(3) Over the past 35 years, the areal average precipitation, runoff and ET in the Yellow River source region were 547 mm, 175 mm and 372 mm, respectively. The annual precipitation first decreased by 58.4 mm per decade from 1981 to 2002 and then increased by 71.1 mm per decade from 2002 to 2015. The annual runoff exhibited a trend similar to that of precipitation, but the runoff coefficient displayed a decreasing trend. The mean air temperature increased significantly by 0.66 °C per decade, and the annual ET increased by 14.3 mm per decade.

(4) Based on the vegetation response at the start of the growing season, the LAI exhibited an increasing trend, with a mean rate of change of 2.1×10^{-3} per year. Additionally, the decreasing frozen ground depth had a positive effect on the LAI, although the most rapid rate of decrease of the frozen ground depth (< -3.0 cm/a) was associated with a decrease in the soil moisture of the upper soil layer; therefore, this change had a negative effect on vegetation growth.

In this study, we did not consider the anthropogenic impacts on hydrological processes and vegetation growth because the model simulated the natural processes driven by historical climatic data. However, the effects of human activities on the water balance components and permafrost degradation can be an important issue as well, and further studies are required to investigate these issues.

Acknowledgements

This research was supported by grants from the National Natural Science Foundation of China (Project Nos. 41630856, 91225302 and 91425303). Y. Qin was supported by a grant from the China Scholarship Council (No. 201606210243) for the study at Lawrence Berkeley National Laboratory. The authors acknowledge the China Meteorological Administration for generously providing the soil temperature and frozen ground depth data in the study area. The authors thank Dr. Barret Kurylyk and an anonymous reviewer for their constructive and detailed comments. The graphical abstract is partly adapted from Li et al. (2015b) and Walvoord and Kurylyk (2016).

References

Bartos and Chester, 2015
M.D. Bartos, M.V. Chester**Impacts of climate change on electric power supply in the Western United States**
Nat. Clim. Chang., 5 (8) (2015), pp. 748-752, 10.1038/nclimate2648
Belmecheri et al., 2016
S. Belmecheri, F. Babst, E.R. Wahl, D.W. Stahle, V. Trouet**Multi-century evaluation of Sierra Nevada snowpack**
Nat. Clim. Chang., 6 (1) (2016), pp. 2-3, 10.1038/nclimate2809
Bense et al., 2012
V.F. Bense, H. Kooi, G. Ferguson, T. Read**Permafrost degradation as a control on hydrogeological regime shifts in a warming climate**
J. Geophys. Res. Earth, 117 (3) (2012), 10.1029/2011JF002143
Bosson et al., 2012
E. Bosson, U. Sabel, L.-G. Gustafsson, M. Sassner, G. Destouni**Influences of shifts in climate, landscape, and permafrost on terrestrial hydrology**
J. Geophys. Res. Atmos., 117 (5) (2012), 10.1029/2011JD016429
Cable et al., 2014
J.M. Cable, K. Ogle, W.R. Bolton, L.P. Bentley, V. Romanovsky, H. Iwata, Y. Harazono, J.Welker**Permafrost thaw affects boreal deciduous plant transpiration through increased soil water, deeper thaw, and warmer soils**
Ecohydrology, 7 (3) (2014), pp. 982-997, 10.1002/eco.1423
Chaves et al., 2017
D.A. Chaves, G.B. Lyra, M.R. Francelino, L.D.B. Silva, A. Thomazini, C. Schaefer**Active layer and permafrost thermal regime in a patterned ground**

soil in Maritime Antarctica, and relationship with climate variability models
Sci. Total Environ., 15 (584-585) (2017), pp. 572-585
Che et al., 2014
M. Che, B. Chen, J.L. Innes, G. Wang, X. Dou, T. Zhou, H. Zhang, J. Yan, G. Xu, H. Zhao**Spatial and temporal variations in the end date of the vegetation growing season throughout the Qinghai–Tibetan Plateau from 1982 to 2011**
Agric. For. Meteorol., 189-190 (2014), pp. 81-90, 10.1016/j.agrformet.2014.01.004
Cheng and Jin, 2013
G. Cheng, H. Jin**Permafrost and groundwater on the Qinghai-Tibet Plateau and in northeast China**
Hydrogeol. J., 21 (1) (2013), pp. 5-23
Cheng and Wu, 2007
G. Cheng, T. Wu**Responses of permafrost to climate change and their environmental significance, Qinghai-Tibet Plateau**
J. Geophys. Res. Earth, 112 (2) (2007), 10.1029/2006JF000631
CMA, 2007
CMA**Specifications for Surface Meteorological Observation, Part14: Measurement of Frozen Soil**
China Meteorological Press, Beijing, China (2007), p. 3
(In Chinese)
Cong et al., 2016
N. Cong, M. Shen, S. Piao**Spatial variations in responses of vegetation autumn phenology to climate change on the Tibetan Plateau**
J. Plant Ecol. (2016), 10.1093/jpe/rtw084
Cong et al., 2009
Z. Cong, D. Yang, B. Gao, H. Yang, H. Hu**Hydrological trend analysis in the Yellow River basin using a distributed hydrological model**
Water Resour. Res., 45 (7) (2009), 10.1029/2008WR006852
Cuo et al., 2015
L. Cuo, Y. Zhang, T.J. Bohn, L. Zhao, J. Li, Q. Liu, B. Zhou**Frozen soil degradation and its effects on surface hydrology in the northern Tibetan Plateau**
J. Geophys. Res. Atmos., 120 (16) (2015), pp. 8276-8298, 10.1002/2015JD023193
Cuo et al., 2013

L. Cuo, Y. Zhang, Y. Gao, Z. Hao, L. Cairang**The impacts of climate change and land cover/use transition on the hydrology in the upper Yellow River basin, China**
J. Hydrol., 502 (2013), pp. 37-52, 10.1016/j.jhydrol.2013.08.003
Dai et al., 2013
Y. Dai, W. Shangguan, Q. Duan, B. Liu, S. Fu, G. Niu**Development of a China dataset of soil hydraulic parameters using Pedotransfer functions for land surface modeling**
J. Hydrometeorol., 14 (3) (2013), pp. 869-887, 10.1175/jhm-d-12-0149.1
Dorji et al., 2013
T. Dorji, Ø. Totland, S.R. Moe, K.A. Hopping, J. Pan, J.A. Klein**Plant functional traits mediate reproductive phenology and success in response to experimental warming and snow addition in Tibet**
Glob. Chang. Biol., 19 (2) (2013), pp. 459-472, 10.1111/gcb.12059
Duan et al., 2017a
L. Duan, X. Man, B. Kurylyk, T. Cai**Increasing winter Baseflow in response to permafrost thaw and precipitation regime shifts in northeastern China**
Water, 9 (1) (2017), p. 25
Duan et al., 2017b
L. Duan, X. Man, B.L. Kurylyk, T. Cai, Q. Li**Distinguishing streamflow trends caused by changes in climate, forest cover, and permafrost in a large watershed in northeastern China**
Hydrol. Process., 31 (10) (2017), pp. 1938-1951, 10.1002/hyp.11160
FAO et al., 2009
FAO, IIASA, ISRIC, ISS-CAS, JRC**Harmonized World Soil Database (Version 1.1). FAO, Rome, Italy and IIASA, Laxenburg, Austria** (2009)
Farouki, 1981
O.T. Farouki**The thermal properties of soils in cold regions**
Cold Reg. Sci. Technol., 5 (1) (1981), pp. 67-75
Flerchinger and Saxton, 1989
G. Flerchinger, K.E. Saxton**Simultaneous heat and water model of a freezing snow-residue-soil system I. Theory and development**
Trans. ASAE, 32 (2) (1989), pp. 0565-0571
Frauenfeld and Zhang, 2011
O.W. Frauenfeld, T. Zhang**An observational 71-year history of seasonally frozen ground changes in the Eurasian high latitudes**
Environ. Res. Lett., 6 (4) (2011), Article 044024

Gao et al., 2016
B. Gao, Y. Qin, Y. Wang, D. Yang, Y. Zheng**Modeling ecohydrological processes and spatial patterns in the Upper Heihe Basin in China**
Forests, 7 (1) (2016), p. 1, 10.3390/f7010010
Gao et al., 2017a
B. Gao, D. Yang, Y. Qin, Y. Wang, H. Li, Y. Zhang, T. Zhang**Change in frozen soils and its effect on regional hydrology in the upper Heihe Basin, the Northeast Qinghai-Tibetan Plateau**
Cryosphere Discuss., 2017 (2017), pp. 1-55, 10.5194/tc-2016-289
Gao et al., 2017b
Z. Gao, F. Niu, Y. Wang, J. Luo, Z. Lin**Impact of a thermokarst lake on the soil hydrological properties in permafrost regions of the Qinghai-Tibet Plateau, China**
Sci. Total Environ., 574 (2017), pp. 751-759, 10.1016/j.scitotenv.2016.09.108
Hu et al., 2011
Y. Hu, S. Maskey, S. Uhlenbrook, H. Zhao**Streamflow trends and climate linkages in the source region of the Yellow River, China**
Hydrol. Process., 25 (22) (2011), pp. 3399-3411, 10.1002/hyp.8069
Huang et al., 2012
J. Huang, X. Guan, F. Ji**Enhanced cold-season warming in semi-arid regions**
Atmos. Chem. Phys., 12 (12) (2012), pp. 5391-5398, 10.5194/acp-12-5391-2012
Hubbard et al., 2013
S.S. Hubbard, C. Gangodagamage, B. Dafflon, H. Wainwright, J. Peterson, A. Gusmeroli, C. Ulrich, Y. Wu, C. Wilson, J. Rowland, C. Tweedie, S.D. Wullschleger**Quantifying and relating land-surface and subsurface variability in permafrost environments using LiDAR and surface geophysical datasets**
Hydrogeol. J., 21 (1) (2013), pp. 149-169
Iijima et al., 2014
Y. Iijima, T. Ohta, A. Kotani, A.N. Fedorov, Y. Kodama, T.C. Maximov**Sap flow changes in relation to permafrost degradation under increasing precipitation in an eastern Siberian larch forest**
Ecohydrology, 7 (2) (2014), pp. 177-187, 10.1002/eco.1366
Immerzeel et al., 2010
W.W. Immerzeel, L.P.H. van Beek, M.F.P. Bierkens**Climate change will affect the Asian water towers**
Science, 328 (5984) (2010), pp. 1382-1385, 10.1126/science.1183188

Jarvis et al., 2008
A. Jarvis, H.I. Reuter, A. Nelson, E. Guevara**Hole-filled seamless SRTM data V4, International Centre for Tropical Agriculture (CIAT)**
(2008)
(Available online: <http://srtm.csi.cgiar.org>)
Jin et al., 2009
H. Jin, R. He, G. Cheng, Q. Wu, S. Wang, L. Lü, X. Chang**Changes in frozen ground in the source area of the Yellow River on the Qinghai–Tibet Plateau, China, and their eco-environmental impacts**
Environ. Res. Lett., 4 (4) (2009), Article 045206
Jin and Li, 2009
R. Jin, X. Li**Improving the estimation of hydrothermal state variables in the active layer of frozen ground by assimilating in situ observations and SSM/I data**
Sci. China Ser. D Earth Sci., 52 (11) (2009), p. 1732, 10.1007/s11430-009-0174-0
Johansen, 1975
O. Johansen**Thermal Conductivity of Soils**
(Ph. D Thesis)
Trondheim University, Trondheim, Norway (1975)
Koren et al., 1999
V. Koren, J. Schaake, K. Mitchell, Q.Y. Duan, F. Chen, J.M. Baker**A parameterization of snowpack and frozen ground intended for NCEP weather and climate models**
J. Geophys. Res. Atmos., 104 (D16) (1999), pp. 19569-19585, 10.1029/1999JD900232
Kurylyk and Watanabe, 2013
B.L. Kurylyk, K. Watanabe**The mathematical representation of freezing and thawing processes in variably-saturated, non-deformable soils**
Adv. Water Resour., 60 (2013), pp. 160-177, 10.1016/j.advwatres.2013.07.016
Li et al., 2012
M. Li, D. Yang, J. Chen, S.S. Hubbard**Calibration of a distributed flood forecasting model with input uncertainty using a Bayesian framework**
Water Resour. Res., 48 (8) (2012), 10.1029/2010WR010062
Li and Cheng, 1996
S. Li, G. Cheng**Map of Frozen Ground on Qinghai-Tibet Plateau**
Gansu Culture Press, Lanzhou, China (1996)

Li et al., 2015a
Z. Li, X. Liu, T. Niu, D. Kejia, Q. Zhou, T. Ma, Y. Gao**Ecological restoration and its effects on a regional climate: the source region of the Yellow River, China**
Environ. Sci. Technol., 49 (10) (2015), pp. 5897-5904, 10.1021/es505985q
Li et al., 2015b
Z. Li, D. Yang, B. Gao, Y. Jiao, Y. Hong, T. Xu**Multiscale hydrologic applications of the latest satellite precipitation products in the Yangtze River basin using a distributed hydrologic model**
J. Hydrometeorol., 16 (1) (2015), pp. 407-426
Luo et al., 2012
D. Luo, H. Jin, L. Lin, R. He, S. Zhang, X. Chang**Degradation of permafrost and cold-environments on the interior and eastern Qinghai Plateau**
J. Glaciol. Geocryol., 34 (3) (2012), pp. 538-546
(In Chinese)
Miao et al., 2016
Q. Miao, D. Yang, H. Yang, Z. Li**Establishing a rainfall threshold for flash flood warnings in China's mountainous areas based on a distributed hydrological model**
J. Hydrol., 541 (Part A) (2016), pp. 371-386, 10.1016/j.jhydrol.2016.04.054
Moriasi et al., 2007
D.N. Moriasi, J.G. Arnold, M.W. Van
Liew, R.L. Bingner, R.D. Harmel, T.L. Veith**Model evaluation guidelines for systematic quantification of accuracy in watershed simulations**
Trans. ASABE, 50 (3) (2007), pp. 885-900
Mu et al., 2015
C. Mu, T. Zhang, Q. Wu, X. Peng, B. Cao, X. Zhang, B. Cao, G. Cheng**Editorial : organic carbon pools in permafrost regions on the Qinghai–Xizang (Tibetan) Plateau**
Cryosphere, 9 (2) (2015), pp. 479-486, 10.5194/tc-9-479-2015
Oleson et al., 2010
K.W. Oleson, D.M. Lawrence, B. Gordon, M.G. Flanner, E. Kluzek, J. Peter, S. L evis, S.C.Swenson, E. Thornton, J. Feddema, C.L. Heald, F. Hoffman, J. Lamarq ue, N. Mahowald, G. Niu, T. Qian, J. Randerson, S. Running, K. Sakaguchi, A. S later, R. Stöckli, A. Wang, Z. Yang, X. Zeng, X. Zeng**Technical Description of Version 4.0 of the Community Land Model (CLM). NCAR Technical Note NCAR/TN-47 + STR**
National Center for Atmospheric Research, Boulder, CO (2010)
(257 pp)

Oliva et al., 2016
M. Oliva, A. Gómez-Ortiz, F. Salvador-Franch, M. Salvà-Catarineu, D. Palacios, L. Tanarro, M.Ramos, P. Pereira, J. Ruiz-Fernández**Inexistence of permafrost at the top of the Veleta peak (Sierra Nevada, Spain)**
Sci. Total Environ., 550 (2016), pp. 484-494, 10.1016/j.scitotenv.2016.01.150
Pang et al., 2012
Q. Pang, L. Zhao, S. Li, Y. Ding**Active layer thickness variations on the Qinghai–Tibet Plateau under the scenarios of climate change**
Environ. Earth Sci., 66 (3) (2012), pp. 849-857, 10.1007/s12665-011-1296-1
Peng et al., 2017
X. Peng, T. Zhang, O.W. Frauenfeld, K. Wang, B. Cao, X. Zhong, H. Su, C. Mu**R esponse of seasonal soil freeze depth to climate change across China**
Cryosphere, 11 (3) (2017), pp. 1059-1073, 10.5194/tc-11-1059-2017
Qin et al., 2016
Y. Qin, H. Lei, D. Yang, B. Gao, Y. Wang, Z. Cong, W. Fan**Long-term change in the depth of seasonally frozen ground and its ecohydrological impacts in the Qilian Mountains, northeastern Tibetan Plateau**
J. Hydrol., 542 (2016), pp. 204-221, 10.1016/j.jhydrol.2016.09.008
Ran et al., 2012
Y. Ran, X. Li, G. Cheng, T. Zhang, Q. Wu, H. Jin, R. Jin**Distribution of permafrost in China: an overview of existing permafrost maps**
Permafr. Periglac. Process., 23 (4) (2012), pp. 322-333, 10.1002/ppp.1756
Rotenberg and Yakir, 2010
E. Rotenberg, D. Yakir**Contribution of semi-arid forests to the climate system**
Science, 327 (5964) (2010), pp. 451-454, 10.1126/science.1179998
Sellers et al., 1996
P.J. Sellers, D.A. Randall, G.J. Collatz, J.A. Berry, C.B. Field, D.A. Dazlich, C. Zh ang, G.D.Collelo, L. Bounoua**A revised land surface parameterization (SiB2) for atmospheric GCMS. Part I: model formulation**
J. Clim., 9 (4) (1996), pp. 676-705
Shen and Xiong, 2016
Y. Shen, A. Xiong**Validation and comparison of a new gauge-based precipitation analysis over mainland China**
Int. J. Climatol., 36 (1) (2016), pp. 252-265, 10.1002/joc.4341
Smith et al., 2007

L.C. Smith, T.M. Pavelsky, G.M. MacDonald, A.I. Shiklomanov, R.B. Lammers**Rising minimum daily flows in northern Eurasian rivers: a growing influence of groundwater in the high-latitude hydrologic cycle**
J. Geophys. Res. Biogeo., 112 (4) (2007), 10.1029/2006JG000327
Stähli et al., 1996
M. Stähli, P.-E. Jansson, L.-C. Lundin**Preferential water flow in a frozen soil—a two-domain model approach**
Hydrol. Process., 10 (10) (1996), pp. 1305-1316
Walvoord and Kurylyk, 2016
M.A. Walvoord, B.L. Kurylyk**Hydrologic impacts of thawing permafrost—a review**
Vadose Zone J., 15 (6) (2016), 10.2136/vzj2016.01.0010
Walvoord and Striegl, 2007
M.A. Walvoord, R.G. Striegl**Increased groundwater to stream discharge from permafrost thawing in the Yukon River basin: potential impacts on lateral export of carbon and nitrogen**
Geophys. Res. Lett., 34 (12) (2007), 10.1029/2007GL030216
Wang et al., 2010
L. Wang, T. Koike, K. Yang, R. Jin, H. Li**Frozen soil parameterization in a distributed biosphere hydrological model**
Hydrol. Earth Syst. Sci., 14 (3) (2010), pp. 557-571, 10.5194/hess-14-557-2010
Wang et al., 2015
Q. Wang, T. Zhang, X. Peng, B. Cao, Q. Wu**Changes of soil thermal regimes in the Heihe River basin over western China**
Arct. Antarct. Alp. Res., 47 (2) (2015), pp. 231-241, 10.1657/AAAR00C-14-012
Woo et al., 2000
M.-k. Woo, P. Marsh, J.W. Pomeroy**Snow, frozen soils and permafrost hydrology in Canada, 1995–1998**
Hydrol. Process., 14 (9) (2000), pp. 1591-1611
Wu et al., 2015
Q. Wu, Y. Hou, H. Yun, Y. Liu**Changes in active-layer thickness and near-surface permafrost between 2002 and 2012 in alpine ecosystems, Qinghai–Xizang (Tibet) Plateau, China**
Glob. Planet. Chang., 124 (2015), pp. 149-155, 10.1016/j.gloplacha.2014.09.002
Yang et al., 2015

D. Yang, B. Gao, Y. Jiao, H. Lei, Y. Zhang, H. Yang, Z. Cong**A distributed scheme developed for eco-hydrological modeling in the upper Heihe River**
Sci. China Earth Sci., 58 (1) (2015), pp. 36-45
Yang et al., 1998
D. Yang, S. Herath, K. Musiake**Development of a geomorphology-based hydrological model for large catchments**
Annu. J. Hydraul. Eng., 42 (1998), pp. 169-174
Yang et al., 2002
D. Yang, S. Herath, K. Musiake**A hillslope-based hydrological model using catchment area and width functions**
Hydrol. Sci. J., 47 (1) (2002), pp. 49-65
Yang et al., 2004
D. Yang, C. Li, H. Hu, Z. Lei, S. Yang, T. Kusuda, T. Koike, K. Musiake**Analysis of water resources variability in the Yellow River of China during the last half century using historical data**
Water Resour. Res., 40 (6) (2004), 10.1029/2003WR002763
Zhang et al., 2009
E. Zhang, C. Gao, Z. Han, J. Ding**Changes of frozen soil in the Yellow River source region and their impact on water resources**
Bull. Geol. Surv. Jpn, 60 (1–2) (2009), pp. 33-38, 10.9795/bullgsj.60.33
Zhang et al., 2015
W. Zhang, Y. Yi, J. Kimball, Y. Kim, K. Song**Climatic controls on spring onset of the Tibetan Plateau Grasslands from 1982 to 2008**
Remote Sens., 7 (12) (2015), p. 15847
Zhang et al., 2007
X. Zhang, S.F. Sun, Y. Xue**Development and testing of a frozen soil parameterization for cold region studies**
J. Hydrometeorol., 8 (4) (2007), pp. 690-701, 10.1175/jhm605.1
Zheng et al., 2009
H. Zheng, L. Zhang, R. Zhu, C. Liu, Y. Sato, Y. Fukushima**Responses of streamflow to climate and land surface change in the headwaters of the Yellow River basin**
Water Resour. Res., 45 (7) (2009), 10.1029/2007WR006665
Zhu et al., 2013
Z. Zhu, J. Bi, Y. Pan, S. Ganguly, A. Anav, L. Xu, A. Samanta, S. Piao, R. Nemani, R. Myneni**Global data sets of vegetation leaf area index (LAI)3g and fraction of Photosynthetically active radiation (FPAR)3g derived from global inventory modeling and mapping studies (GIMMS)**

normalized difference vegetation index (NDVI3g) for the period 1981 to 2011

Remote Sens., 5 (2) (2013), p. 927, 10.3390/rs5020927